ENG. Struct. Civ. Eng. 2026, 20(3): 493–506
https://doi.org/10.1007/s11709-026-1296-6

RESEARCH ARTICLE

Discarded mask fiber-glass powder composite enhanced microbially induced calcite precipitation-treated calcareous sand: Mechanical property and micro-mechanism

Zhanpeng JI[a], Xinlei ZHANG[a,b*], Lu LIU[a,b], Xuanxuan LIU[a], Hongmei GAO[a,b], Zhihua WANG[a,b], Jun ZHOU[c]

[a] *Urban Underground Space Research Center, Nanjing Tech University, Nanjing 211816, China*

[b] *Jiangsu Province Engineering Research Center of Transportation Infrastructure Security Technology, Nanjing Tech University, Nanjing 211816, China*

[c] *College of Biotechnology and Pharmaceutical Engineering, Nanjing Tech University, Nanjing 211816, China*

[*] *Corresponding author. E-mail: xinlei.zhang@njtech.edu.cn*

ABSTRACT The low bearing capacity of calcareous sand challenges island reef engineering. While microbially induced calcite precipitation (MICP) is an emerging reinforcement method, it suffers from brittleness and low mineralization efficiency. This study proposes a novel composite strategy combining MICP with discarded mask fibers (DMF) and waste glass powder (GP) to address these limitations. Both DMF and GP individually boost microbial mineralization by offering nucleation sites, enhancing bacterial retention, and improving Ca^{2+} utilization. The composite system significantly outperformed pure MICP. Optimal strength was achieved at a ratio of 6 mm 0.2% DMF and 13 μm 4% GP (by weight of sand), yielding a maximum unconfined compressive strength (UCS) of 1327 kPa. This is a 136% increase in UCS and a 143% increase in the toughness index over the MICP-only group. Furthermore, the synergy improved deformation performance, with the deformation index surging by 396% under 12 mm 0.2% DMF and 13 μm 4% GP. GP particles fill voids to densify the cementation matrix, while the DMF network provides bridging action, enhancing ductility. Microstructural analysis confirms a robust framework of dense GP-$CaCO_3$ clusters interconnected by the DMF network. This research presents a novel, sustainable solution utilizing upcycled waste for island reef construction.

KEYWORDS calcareous sand, mechanical property, MICP, DMF, GP, micro-mechanism

1 Introduction

Calcareous sand, an abundant resource in tropical marine regions, is a key fill material used in offshore reclamation and the building of island reefs. However, its biogenic origin, derived from the weathered fragments of marine life, including corals and shells, endows it with inherently problematic engineering properties [1–3]. These include high intraparticle porosity, extreme particle irregularity, significant crushability, and low natural bearing capacity [4–7]. Consequently, foundations built on untreated calcareous sand are prone to excessive post-construction settlement, rendering them unable to meet essential bearing capacity and stability requirements [8]. As such, ground improvement techniques are indispensable for enhancing its mechanical performance.

Microbially induced calcite precipitation (MICP) has emerged as an effective ground improvement approach for these foundations, garnering considerable attention in geotechnical engineering for its environmental sustainability, low energy consumption, and minimal site disturbance [9–14]. While the $CaCO_3$ cementation induced by MICP effectively bonds sand particles to improve strength, stiffness, and resistance to liquefaction

Article history: Received Oct 17, 2025; Accepted Nov 22, 2025

[15–18], two significant challenges hinder its practical application. First, the treated sand often exhibits undesirable brittle fracture behavior [19–21], which compromises its deformation tolerance. Second, the low bacterial adsorption efficiency on the highly porous calcareous substrate results in an inefficient and non-uniform distribution of $CaCO_3$ [22], necessitating costly and time-consuming multi-phase treatments [23,24]. These limitations currently restrict the field-scale deployment of MICP in critical infrastructure projects.

Numerous scholars are dedicated to improving MICP reinforcement technology to enhance its efficiency and material performance to overcome these limitations. Xiao et al. [25] utilized microfluidic chips to visualize the heterogeneous growth mechanisms of $CaCO_3$ crystals and bacterial distribution during MICP, finding that low calcium chloride ($CaCl_2$) concentrations contribute to more uniform bacterial diffusion. Furthermore, Zhao et al. [26] demonstrated that optimizing urease and cementing solution concentrations, particularly lower cementing solution levels, can enhance MICP crystal uniformity and efficiency. Banik and Sarkar [27] conducted consolidated undrained cyclic triaxial testing on MICP-treated sand to evaluate the effects of different bacterial strains, treatment duration, and wetting–drying cycles on the shear modulus and damping ratio. Xiao et al. [28] demonstrated that combining bio-hydrogel and MICP treatment significantly improved the water retention capacity and surface strength of sand. However, despite significant progress in process refinement [29,30], single process optimization methods still face challenges in thoroughly addressing the brittle behavior of treated sand and the low bacterial adsorption efficiency.

Simultaneously, the proliferation of discarded face masks presents a severe environmental threat. Their primary component, polypropylene (PP) fibers from materials like melt-blown fabric, exhibits high chemical stability and remarkable resistance to natural degradation [31]. Reports from international environmental organizations estimate that 15.6 billion masks entered marine ecosystems globally in 2020 alone, contributing between 1680 and 6240 t of plastic waste [32,33]. A similar challenge is posed by industrial waste glass, whose high physical inertness and low recyclability make it a significant solid waste concern. Paradoxically, the properties of these waste materials offer synergistic solutions to the aforementioned limitations of MICP. PP fibers derived from masks can enhance the ductility of treated sand, mitigating the brittle failure commonly observed in MICP-treated calcareous sand. Concurrently, glass powder (GP) from milled industrial waste improves bacterial adsorption via micron-scale pore filling, addressing key challenges of reinforcement efficiency and uniformity while promoting sustainable material reuse.

It is well-established that fiber and powder materials offer distinct advantages for reinforcement and filling applications in geotechnical engineering [34–36]. Specifically, in the domain of combined fiber-MICP reinforcement, existing research demonstrates that the synergy between fiber reinforcement and microbial mineralization can substantially enhance soil properties. Han et al. [37] introduced PP fibers from waste masks and observed a near 100% increase in unconfined compressive strength (UCS) compared to fiber-free specimens, attributing this to the bridging effect of fibers across the cementation structure. Tang et al. [38] found that $CaCO_3$ crystal production increased with fiber dosage. Their scanning electron microscope (SEM) analysis revealed continuous cementation layers on fiber surfaces, confirming that fibers act as nucleation sites for bacterial adsorption and mineralization. For powder-MICP combined reinforcement, Zhao et al. [39] conducted studies on silica powder-MICP-treated medium-coarse sand, finding that a 3% mass dosage of silica powder increased bacterial activity retention to 43.5%, and $CaCO_3$ production by 180%, while the dry UCS reached 1.12 MPa (three times higher than the control group). However, the incorporation of powder significantly increased the brittleness of the reinforced system [40].

While the benefits of incorporating single additives into MICP-treated soil are well-documented, research has yet to explore the synergistic effects of composite systems. This study is the first to systematically investigate the use of both discarded mask fibers (DMF) and waste GP to reinforce MICP-treated calcareous sand. Through a series of comparative experiments, key parameters, including bacterial adsorption rates (BARs), Ca^{2+} utilization, and UCS, are quantified. Microstructural analyses using X-ray diffraction (XRD) and SEM were also performed to examine the influence of additive type, dosage, and size on microbial mineralization, calcium carbonate crystal evolution, and overall mechanical performance. By integrating these results, this study elucidates the underlying mechanism by which the DMF-GP composite enhances MICP treatment, providing a theoretical and experimental foundation for developing efficient, eco-friendly ground improvement technologies.

2 Materials and methods

2.1 Materials

2.1.1 Calcareous sand

The calcareous sand utilized in this study, sourced from a reef area in the South China Sea, is a typical biogenic sediment. Its mineralogical composition, as determined

by XRD analysis, is predominantly calcium carbonate (> 90%), with aragonite, high-magnesium calcite (Mg-calcite), and calcite as the primary constituents [17]. Before testing, the sand was sieved to retain particles smaller than 1 mm, and the resulting grain size distribution is presented in Fig. 1. Its key physical properties were determined according to ASTM standards [41]. The mean particle size (d_{50}) is 0.33 mm, the effective particle size (d_{10}) is 0.16 mm, the maximum void ratio (e_{max}) is 1.15, the minimum void ratio (e_{min}) is 0.65, and the specific gravity (G_S) is 2.80. The sand is classified as a poorly graded sand based on the coefficient of uniformity (C_u), which is 2.26, and the coefficient of curvature (C_c), which is 1.12.

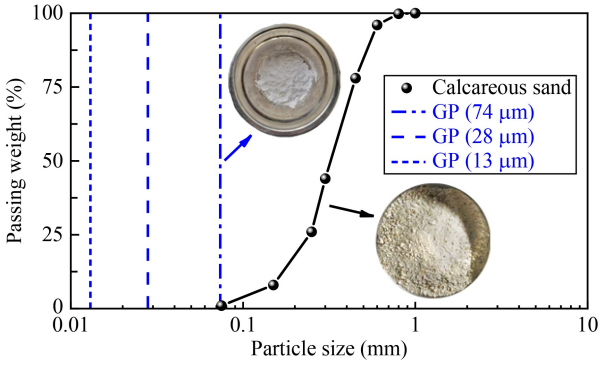

Fig. 1 Calcareous sand particle size distribution and GP particle size.

2.1.2 Glass powder and discarded mask fiber

The GP used in this study was derived from waste soda-lime glass. The GP was prepared through a two-stage comminution process, beginning with coarse crushing of waste soda-lime glass in a jaw crusher and concluding with fine grinding in a planetary ball mill. Subsequent sieving yielded three distinct, narrowly graded fractions. For this study, the particle sizes of these fractions, namely 74, 28, and 13 μm (corresponding to 200-mesh, 500-mesh, and 1000-mesh standard sieves, respectively), were characterized solely by the nominal apertures of the standard sieves employed. X-ray fluorescence (XRF) analysis revealed the primary chemical composition of the GP to be SiO_2 (69.2 wt.%), Na_2O (11.4 wt%), CaO (9.5 wt%), Al_2O_3 (3.4 wt%), and MgO (2.5 wt%) [42,43]. The GP had a specific gravity of 2.73. Its ultrafine particle size (13–74 μm) creates a high specific surface area, which enhances interfacial contact with the sand grains. This, in turn, facilitates microbial colonization and subsequent bio-cementation during the MICP process.

The DMF utilized in this study were sourced from single-use medical masks, which consist of two outer spunbond non-woven layers and an inner melt-blown PP fabric layer [44]. The melt-blown fabric, serving as the core filtration medium, consists of ultrafine PP fibers featuring extensive specific surface areas and strong adsorption capabilities. To ensure sterility and compliance with testing standards, the collected masks first underwent a decontamination process, being dried in an oven at 105 °C for 24 h. This thermal treatment was confirmed not to significantly alter the mechanical properties of the fibers [45]. Subsequently, the metal strips and non-woven layers were manually removed from the dried masks to eliminate non-fiber impurities that might interfere with experimental results. For fiber preparation, the melt-blown PP layer of the mask was cut into strips with a width of 1 mm, which were then further trimmed into fibers with target lengths of 3, 6, 9, 12, and 15 mm. After the cutting process, the prepared DMF was dried again in an oven at 50 °C for 6 h to remove any residual moisture adsorbed during handling.

2.1.3 Bacteria and cementation media

The ureolytic bacterium Sporosarcina pasteurii (ATCC 11859) was selected to catalyze the hydrolysis of urea [46,47]. The bacteria were cultivated in a liquid medium, the composition of which is detailed in Table 1. Before inoculation, the medium's pH was adjusted to 9.0 with 1 M NaOH. Bacterial solution was inoculated into the sterile medium at a 1:10 volume ratio and incubated for 24 h at 30 °C with continuous agitation at 210 r/min in a thermostatic shaker. The resultant bacterial culture reached an optical density (OD_{600}) of 1.3 and exhibited a urease activity of 2.4 $mmol \cdot L^{-1} \cdot min^{-1}$. These parameters confirmed the culture's high activity and suitability for the subsequent MICP reinforcement experiments.

Table 1 Composition of culture medium

Reagent	Concentration
Yeast extract	20 g/L
NH_4Cl	10 g/L
$MnCl_2 \cdot 6H_2O$	24 mg/L
$MnSO_4 \cdot H_2O$	10 mg/L
Distilled water	1000 g/L

The cementation solution (CS) is the core reaction medium for the MICP process. It provides both the urea substrate for enzymatic hydrolysis and the calcium ions (Ca^{2+}) required for $CaCO_3$ mineralization, while also offering nutritional support for bacterial metabolic activity [48–50]. For this study, the CS consisted of an equimolar solution of urea and $CaCl_2$ at a concentration of 0.5 M. This specific concentration and 1:1 molar ratio were selected to ensure a balanced supply of substrate for urease catalysis and calcium for carbonate precipitation.

2.2 Sample treatment

Three types of composite mixtures were prepared for this study by uniformly blending dry sand with varying dosages of either DMF, GP, or a combination of both. Each mixture was then carefully layered and compacted into a custom-designed, separable polyvinyl chloride (PVC) mold (internal dimensions: 40 mm diameter × 80 mm height, Fig. 2(a)) to achieve a uniform initial density. The mold assembly consisted of a PVC pedestal and two semi-circular segments, designed to preserve specimen integrity upon removal.

All MICP treatments were conducted at a controlled ambient temperature of 25 °C. The multi-stage grouting procedure, illustrated schematically in Figs. 2(b) and 2(c), involved a repeating cycle. The cycle began with the top-down injection of 75 mL of bacterial suspension using a peristaltic pump at a constant rate of 2 mL/min. A 6-h retention period was then observed to allow for sufficient bacterial adsorption onto the solid matrix. Following this, 75 mL of the CS was injected at the same flow rate. The specimen was then left undisturbed for a 12-h curing period to facilitate $CaCO_3$ precipitation. This entire injection and curing cycle was repeated six times to achieve the desired level of cementation.

Upon completion of the six treatment cycles, any residual salts and unreacted reagents were removed by flushing the specimen twice with 200 mL of deionized water at a flow rate of 2 mL/min.

2.3 Test method

2.3.1 Bacterial adsorption rate

The efficacy of MICP is critically dependent on the adsorption of bacteria onto sand particles [40,51]. This complex process is governed by a multitude of physicochemical interactions, which are, in turn, influenced by factors such as the sand's surface properties, its pore network structure, solution chemistry, and the intrinsic characteristics of the bacteria. Therefore, BARs were systematically measured to investigate how DMF and GP modulate this critical parameter. The results provide fundamental insights and empirical data essential for optimizing MICP technology and advancing its reinforcement efficiency. The BAR was determined as per Eq. (1) [51]:

$$\mathrm{BAR} = \frac{M_1 - M_2}{M_1} \times 100\%, \tag{1}$$

where M_1 and M_2 represent the OD_{600} of the bacterial suspension before and after passing through the specimen and a subsequent retention period, respectively.

2.3.2 Calcium ion utilization rate

The calcium ion utilization rate (S) is a key metric for evaluating the efficacy of the MICP mineralization efficiency. The concentration of Ca^{2+} in solution was determined by EDTA titration [37]. The utilization rate was then calculated using the following expression:

$$S = \left(1 - \frac{c_0 a V_1}{c_1 b V_0}\right) \times 100\%, \tag{2}$$

where c_0 is the molar concentrations (M) of the EDTA titrant; c_1 is the molar concentrations (M) of $CaCl_2$ in the CS; a is the volume (mL) of the EDTA titrant consumed, while b is the volume (mL) of the CS used. V_0 represents the initial volume (mL) of the CS, and V_1 is its final volume (mL) after preparation for titration.

2.3.3 Unconfined compressive strength test

The UCS of the specimens was measured using a SANS microcomputer-controlled electronic compression testing machine. A constant loading rate of 1 mm/min was applied during the UCS tests [52,53]. The resulting pressure and displacement were continuously documented. The UCS test was terminated based on explicit criteria to define the failure point. Specifically, loading

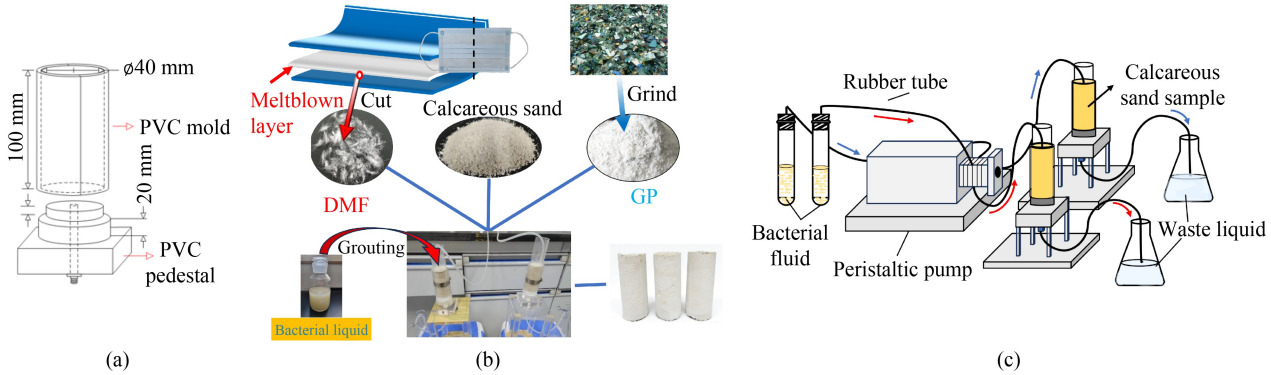

Fig. 2 Grouting process and device schematic diagram: (a) reinforcement mold; (b) incorporation sequence in treatment; (c) treatment process.

was stopped when the axial strain of the specimen reached 20% [54], or when the applied load dropped to below 80% of the peak load, whichever occurred first.

The study was divided into four main groups: a control group (only MICP-treated sand), a single-additive group with DMF (D-M), a single-additive group with GP (G-M), and a composite group with both DMF and GP (D-G-M). In the single-additive series, the influence of DMF was investigated at dosages of 0.1%, 0.2%, 0.3%, and 0.4% (by mass of sand) and at lengths of 3, 6, 9, 12, and 15 mm. Similarly, the effect of GP was tested at dosages of 2%, 4%, and 8% and with particle sizes of 74, 28, and 13 μm. For the composite reinforcement tests, the design was based on the optimal parameters obtained from the single-additive experiments. The fiber parameters were kept fixed while varying either the GP dosage or its particle size to study their synergistic interactions. All specimens were subjected to the consistent MICP treatment protocol at an initial relative density of approximately 50%. The detailed test conditions for all groups are listed in Table 2.

2.3.4 X-ray diffraction test and scanning electron microscope test

XRD analysis was performed to identify the crystalline phases of the precipitated $CaCO_3$ and to evaluate the influence of the incorporated additives (DMF and GP) on mineralogy. Following the UCS tests, fragments from the core of each specimen were collected and ground into a fine powder (particle size < 100 μm) for analysis. The XRD patterns were collected over a 2θ range of 10° to 70° with a scanning speed of 4°/min and a step size of 0.01°. The identification of mineral phases and the estimation of their relative dosages were conducted by analyzing the resulting diffraction patterns, allowing for a quantitative assessment of the additives' impact on crystal formation [55].

SEM was employed to investigate the microstructural characteristics of the reinforced specimens. Four distinct sample types were selected for analysis, corresponding to the main experimental groups. The primary objectives were to examine the morphology and distribution of the precipitated $CaCO_3$, its bonding with the sand grains, and its interaction with the incorporated fibers (DMF and GP).

3 Influence of incorporated materials on MICP process

3.1 Bacterial adsorption rate

The influence of different additives on the BAR within the calcareous sand specimens is presented in Fig. 3. As shown in Fig. 3(a), the BAR is significantly influenced by both the length and dosage of DMF. As the fiber length increased, the BAR exhibited a trend of initially rising and then declining, consistently peaking at a fiber length of 6 mm. This trend suggests that while increasing fiber length up to a certain point (6 mm) enhances bacterial adsorption, further increases beyond this threshold diminish the effect. A possible explanation is that shorter fibers provide a limited surface area for bacterial attachment, resulting in lower adsorption rates. Conversely, excessively long fibers (> 6 mm) are prone to curling, tangling, and agglomeration, which reduces their effective contact area with bacteria and consequently lowers the BAR. Furthermore, DMF dosage also played a crucial role. At dosages below 0.2%, the BAR rose with increasing fiber dosage. However, when the dosage exceeded 0.2%, excessive fibers may have exacerbated agglomeration between sand particles, thereby decreasing the adsorption rate.

The effect of GP on the BAR is illustrated in Fig. 3(b). The results indicate that the BAR progressively increased as the particle size of the GP decreased. This can be attributed to the higher specific surface area of finer GP particles, which allows them to uniformly fill micropores between sand grains and adhere to their surfaces, thereby providing more nucleation sites for bacterial attachment. The GP dosage also had a notable impact. At lower dosages (< 4%), GP was distributed relatively uniformly, effectively increasing the surface roughness of the sand

Table 2 Unconfined compression test condition

Test group	Variable type	Specific parameter
MICP	–	–
D-M	dosage	0.1%, 0.2%, 0.3%, 0.4%
	length	3, 6, 9, 12, and 15 mm
G-M	dosage	2%, 4%, 8%
	particle size	74, 28, and 13 μm
D-G-M	GP dosage	DMF: 0.2% (6 mm) GP：2%/4%/8% (13 μm)
	GP dosage	DMF: 0.4% (12 mm) GP：2%/4%/8% (13 μm)
	GP particle Size	DMF: 0.2% (6 mm) GP：4% (74, 28, and 13 μm)

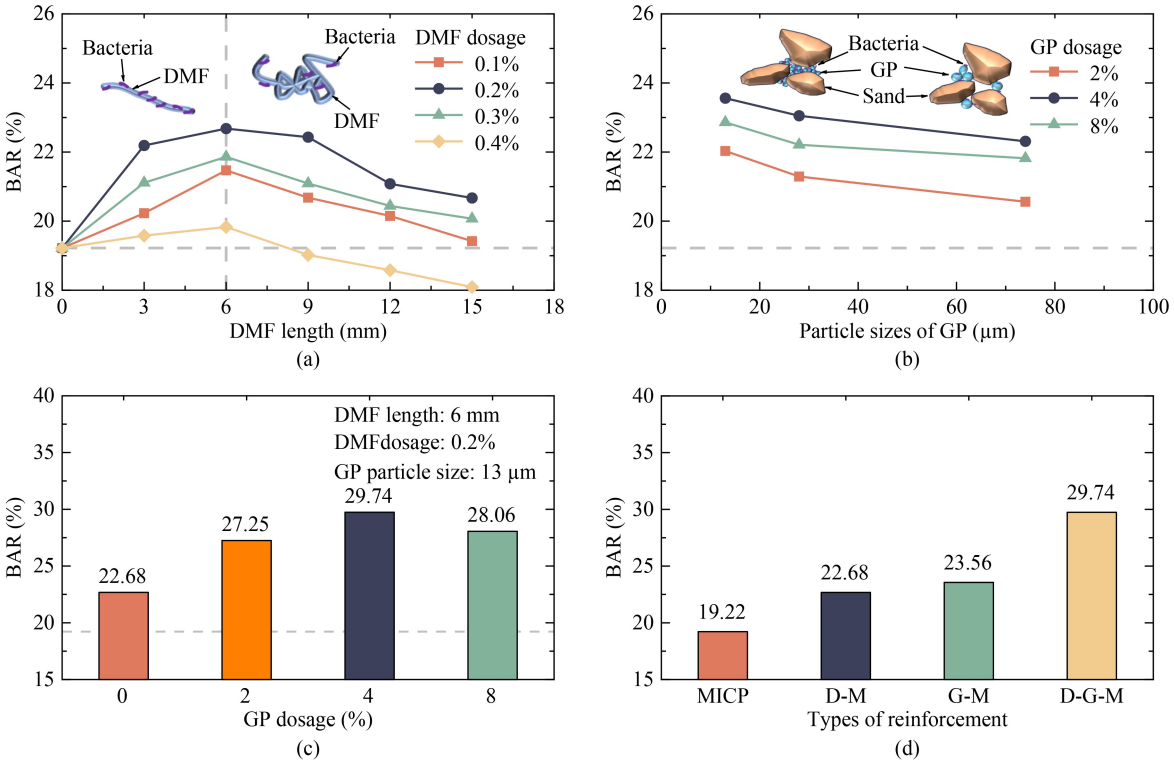

Fig. 3 BAR of samples under different incorporation types: (a) D-M group; (b) G-M group; (c) D-G-M group; (d) optimal incorporation results.

grains and promoting bacterial adsorption. However, at higher dosages (> 4%), an excess of GP may have clogged some pore throats of the sand sample, significantly reduced the specimen's permeability, and impeded the transport and subsequent adsorption of bacteria. This interpretation was later corroborated by SEM microstructural observations.

Figure 3(c) presents the BAR values measured for the D-G-M group. The maximum BAR of 29.74% was achieved at a GP dosage of 4%. This result indicates that the combined incorporation of DMF and GP effectively promotes microbial adsorption within the calcareous sand matrix. A comparison of the optimal BAR values across the four main experimental series is presented in Fig. 3(d). The highest BAR (29.74%) was observed in the composite D-G-M group. The single-additive G-M and D-M groups exhibited comparable but lower rates at 23.56% and 22.68%, respectively. The lowest BAR (19.22%) was recorded for the control group (only MICP). These findings conclusively demonstrate that the rational incorporation of GP and DMF can significantly enhance the BAR in calcareous sand. This suggests that a composite reinforcement approach holds the promise for a more effective MICP treatment outcome.

3.2 Calcium ions utilization rate

The Ca^{2+} utilization rates for all experimental series were presented in Fig. 4. A consistent trend across all groups

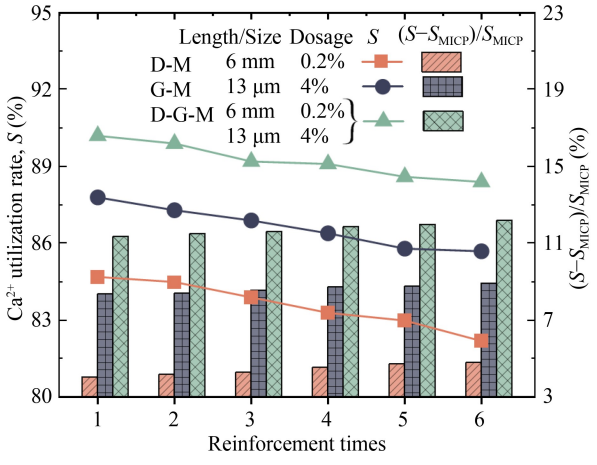

Fig. 4 Calcium ion utilization rate of samples under different incorporation types.

was a gradual decline in Ca^{2+} utilization with an increasing number of treatment cycles. The utilization of Ca^{2+} depends on the continuous activity of the urease-producing bacteria and their effective contact with the CS. With each cycle, the newly precipitated $CaCO_3$ coats the sand grains and partially encapsulates the bacterial cells. This encapsulation limits mass transfer of Ca^{2+} to the reaction sites, which effectively reduces the reactive contact area and slows down the reaction, hence resulting in a decrease in utilization efficiency [56]. The control group (only MICP) demonstrated the lowest utilization

rate at approximately 80%. The addition of either DMF or GP resulted in a significant increase in Ca^{2+} utilization. The highest utilization rate, approximately 90%, was achieved by the composite D-G-M group. Furthermore, the improvement in Ca^{2+} utilization for the D-G-M group, relative to the only MICP control group, was more pronounced than that observed for the single-additive DMF or GP groups. This suggests a synergistic interaction between the fibers and powder, which improves the specimen's capacity to adsorb bacteria and subsequently capture and utilize Ca^{2+} for mineralization.

3.3 Calcium carbonate crystallization characteristics

Figure 5 presents the XRD patterns and calcium carbonate crystal compositions of optimally reinforced specimens under various admixture incorporation strategies. The only MICP control group's diffraction pattern exclusively showed characteristic peaks for aragonite (A) (69.86% mass fraction) and calcite (C) (30.14%), indicating that MICP under these conditions predominantly forms metastable aragonite. Incorporating only GP led to the emergence of a vaterite (V) diffraction peak. Simultaneously, aragonite dosage decreased to 54.11%, calcite slightly increased to 34.37%, and vaterite accounted for 11.52% of the crystalline phases. This suggests that GP alters the crystal growth environment, favoring the formation of thermodynamically unstable vaterite. For specimens incorporating only DMF, the aragonite mass fraction further decreased to 47.73%, calcite increased to 36.53%, and the vaterite dosage rose to 15.74%. This outcome indicates that DMF more significantly promotes vaterite formation compared to GP.

Notably, the co-incorporation of GP and DMF resulted in calcite becoming the predominant crystalline phase (43.58%), surpassing aragonite. Vaterite dosage further increased to 21.33%, while the aragonite proportion decreased to 35.09%. These results demonstrate that the synergy between the two admixtures significantly modulates the crystal precipitation pattern, preferentially forming calcite, the thermodynamically most stable polymorph and mechanically superior polymorph, as the dominant crystalline product.

This preference for calcite with GP and DMF co-incorporation is explained by two primary mechanisms: more efficient bacterial adsorption (Fig. 3) and enhanced Ca^{2+} utilization (Fig. 4). The increased bacterial adsorption offers a higher density of nucleation sites essential for calcium carbonate precipitation. Simultaneously, improved Ca^{2+} utilization ensures a sustained ion supply, creating conditions conducive to preferential calcite precipitation. Additionally, the synergistic effect of GP filling inter-particle voids and DMF providing a fibrous scaffold refines the precipitation environment, thereby promoting crystallization into calcite, the most stable polymorph owing to its lower energy state.

4 Mechanical performance improvement effect

4.1 Unconfined compressive strength

Figure 6 illustrates the influence of various admixtures on

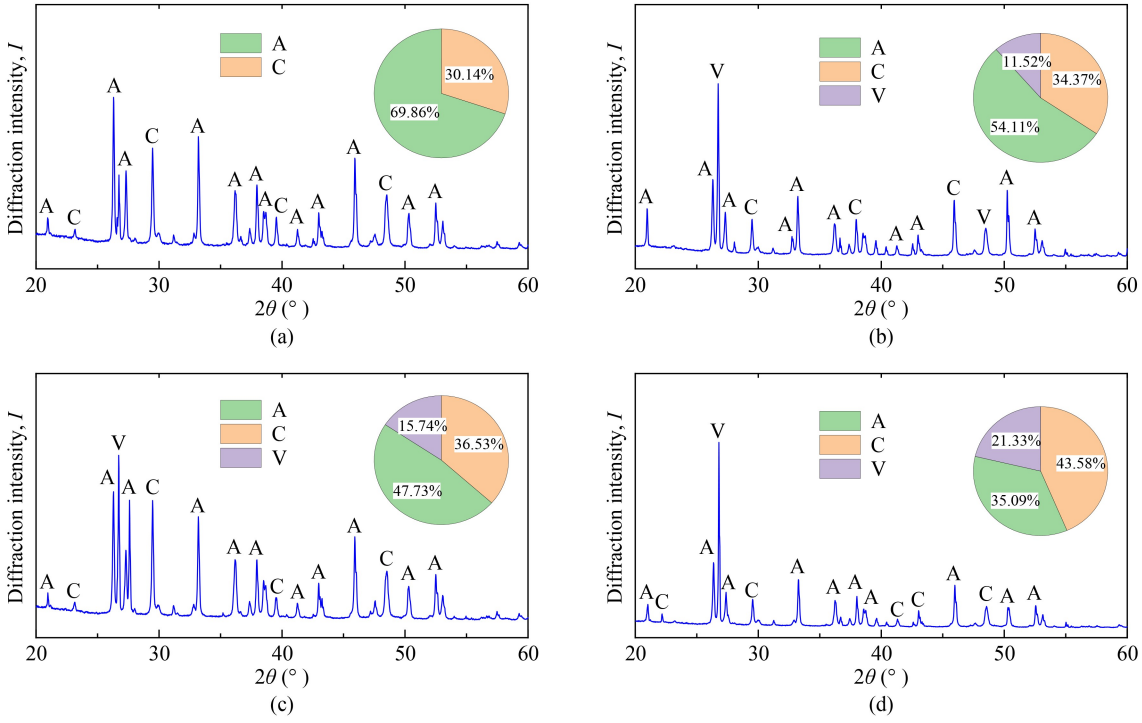

Fig. 5 XRD patterns of samples under different incorporation types: (a) MICP group; (b) G-M group; (c) D-M group; (d) D-G-M group.

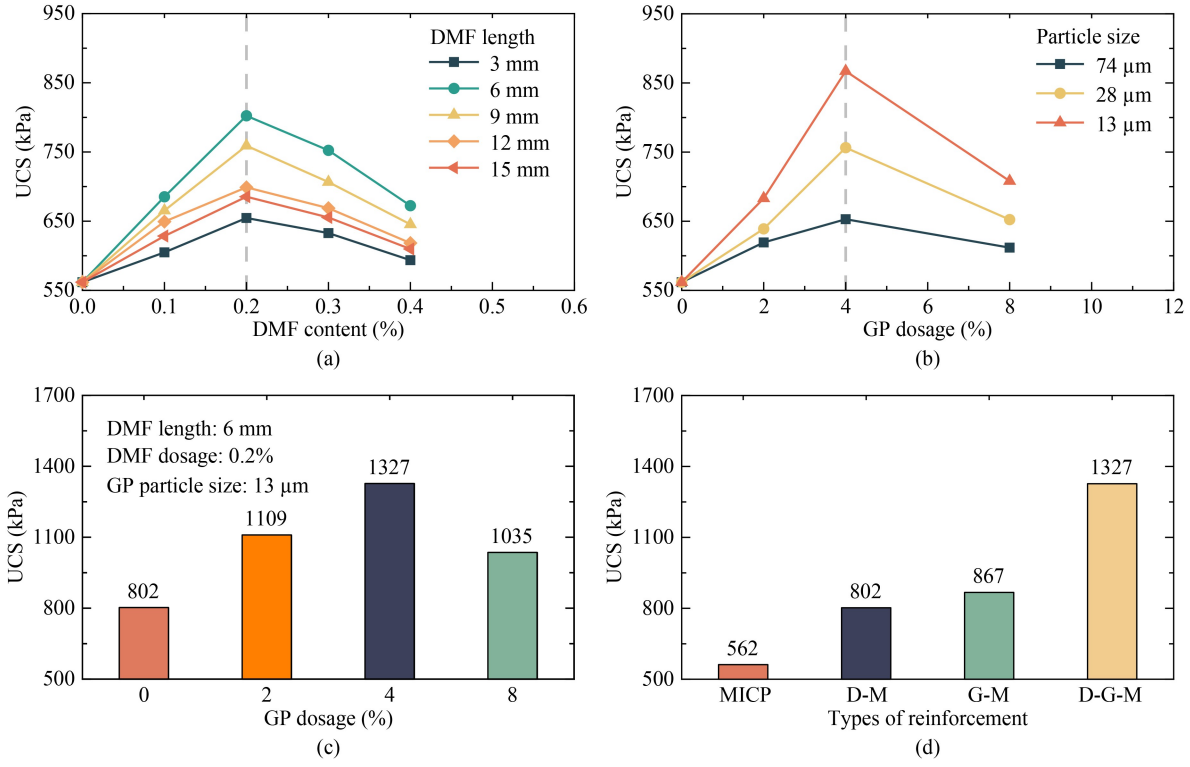

Fig. 6 Effect of incorporation types on UCS of MICP-treated calcareous sand: (a) D-M group; (b) G-M group; (c) D-G-M group; (d) optimal incorporation results.

the UCS of MICP-treated calcareous sand. As shown in Fig. 6(a), for all considered fiber length conditions, when the dosage of DMF reached 0.2%, the specimens exhibited optimal reinforcement and achieved maximum UCS. At a given fiber dosage, specimens reinforced with 6mm fibers demonstrated the highest UCS. This finding is consistent with the previously observed trend in bacterial solution adsorption rates, suggesting a strong correlation between the BAR and the resulting strength of the treatment specimens.

The particle size of GP significantly influences the specimen UCS (Fig. 6(b)). A peak UCS of 867 kPa was achieved with 13 μm GP at a 4% dosage, marking a 54.3% improvement over the only MICP control and substantially outperforming specimens treated with GP grain sizes of 28 and 74 μm. The efficacy of GP stems from its ability to fill inter-granular micro-pores and adsorb onto sand grain surfaces. These mechanisms increase the surface area for microbial attachment and offer more nucleation sites for microbially induced calcium carbonate precipitation, thus improving inter-granular cementation. Conversely, GP dosage above 4% resulted in excessive particle accumulation, causing pore clogging and reduced bacterial adsorption, which ultimately diminishing the UCS strengthening effect.

Specimens treated with a combination of GP and DMF demonstrated a UCS that initially increased with GP dosage, reaching a maximum of 1327 kPa when the GP dosage was 4%, and then gradually decreased. Figure 6(d) highlights the optimal UCS values under various admixture conditions. Specimens treated solely with MICP had a significantly lower UCS of only 562 kPa. The UCS for specimens with only DMF was 802 kPa, and for those with only GP, it was 867 kPa. Notably, the combined incorporation of GP and mask fibers with MICP (D-G-M) yielded the highest UCS at 1327 kPa, which is 2.36 times greater than specimens treated with MICP alone. This pronounced enhancement in mechanical strength is ascribed to a synergistic effect involving two key contributions: first, DMF provides a fibrous scaffold that bridges particles and facilitates calcium carbonate cementation; secondly, GP acts as a filler for inter-granular pores and adsorbs onto particle surfaces, thereby augmenting the effective area for cementation. Critically, these materials work in concert to promote bacterial adsorption and optimize Ca^{2+} utilization. This synergy favors the precipitation of calcite, the crystalline phase of calcium carbonate recognized for its superior mechanical characteristics, ultimately leading to a more robust inter-particle cementation.

4.2 Deformation index

The influence of different admixtures on the deformation index of microbially induced calcareous sand is illustrated in Fig. 7. The deformation index (D) quantifies the change in strain capacity, defined as the ratio of the axial strain at peak unconfined compressive stress for

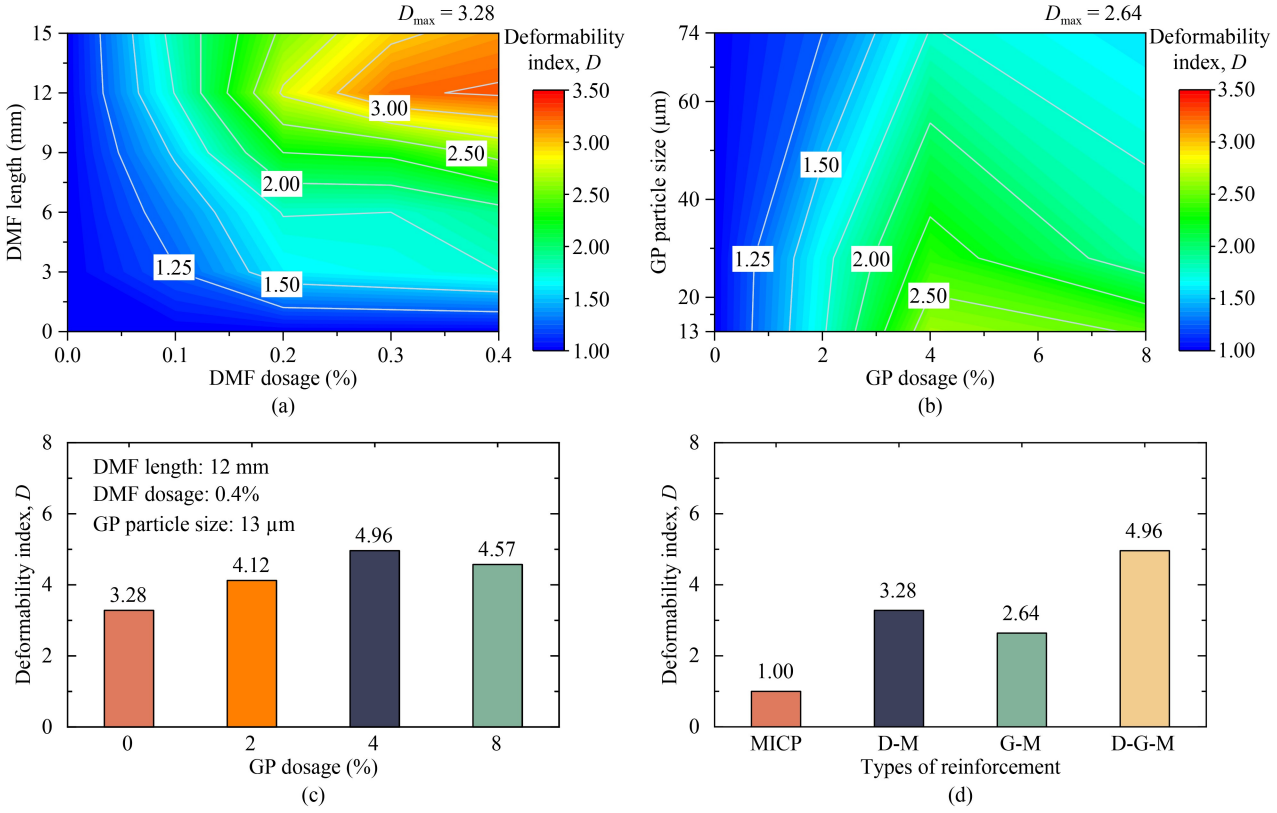

Fig. 7 Effect of incorporation types on deformation index of MICP-treated calcareous sand: (a) D-M group; (b) G-M group; (c) D-G-M group; (d) optimal incorporation results.

specimens containing DMF or GP to that of specimens treated only with MICP. The results indicate that increasing the DMF dosage progressively led to a higher deformation index, with a maximum D value of 3.28 observed for specimens reinforced with 0.4% fiber dosage. Conversely, with increasing GP dosage, the D first increased and then decreased, reaching a peak of 2.64 at a GP dosage of 4%.

Notably, the concurrent incorporation of DMF and GP yielded a D of 4.96 for treated specimens, significantly superior to those reinforced with either DMF or GP individually, or with MICP alone. This improvement in deformation capacity is ascribed to the formation of a flexible bridging network by the DMF, coupled with enhanced cementation provided by an appropriate dosage of GP.

4.3 Toughness index

Toughness serves as a comprehensive parameter reflecting both the strength and deformation capacity of a material. The toughness index (T) quantifies the energy absorption capacity of a material before failure upon reaching its peak stress under applied load. It is determined by integrating the area under the stress–strain curve:

$$T = \int_0^{J_a} \sigma \mathrm{d}\varepsilon \cdot V, \tag{3}$$

where σ is the axial stress, ε is the axial strain, ε_f is the axial strain at final failure, and V is the volume of the test sample.

Figure 8 shows the influence of admixtures on the specimen's T. A maximum T of 76.32 kN·mm was achieved when DMF with a length of 6 mm were incorporated at a dosage of 0.2%. The inclusion of fibers with suitable dimensions and dosage facilitates the formation of an effective, flexible bridging network. When subjected to load, these fibers dissipate energy via mechanisms such as tensile stretching and slippage, thereby enabling the specimen to attain a higher peak strain. It was also observed that the incorporation of GP alone can enhance the specimen's T. Furthermore, Figs. 8(c) and 8(d) demonstrate that the simultaneous incorporation of GP and DMF can significantly enhance the specimen's toughness, achieving mechanical properties that are both strong and ductile, as well as tough without compromising strength.

5 Micromorphological analysis

Figure 9 displays SEM images of treated specimens incorporating various admixtures, aimed at elucidating the regulatory mechanisms of these admixtures on cementation morphology during microbial-induced calcium carbonate precipitation.

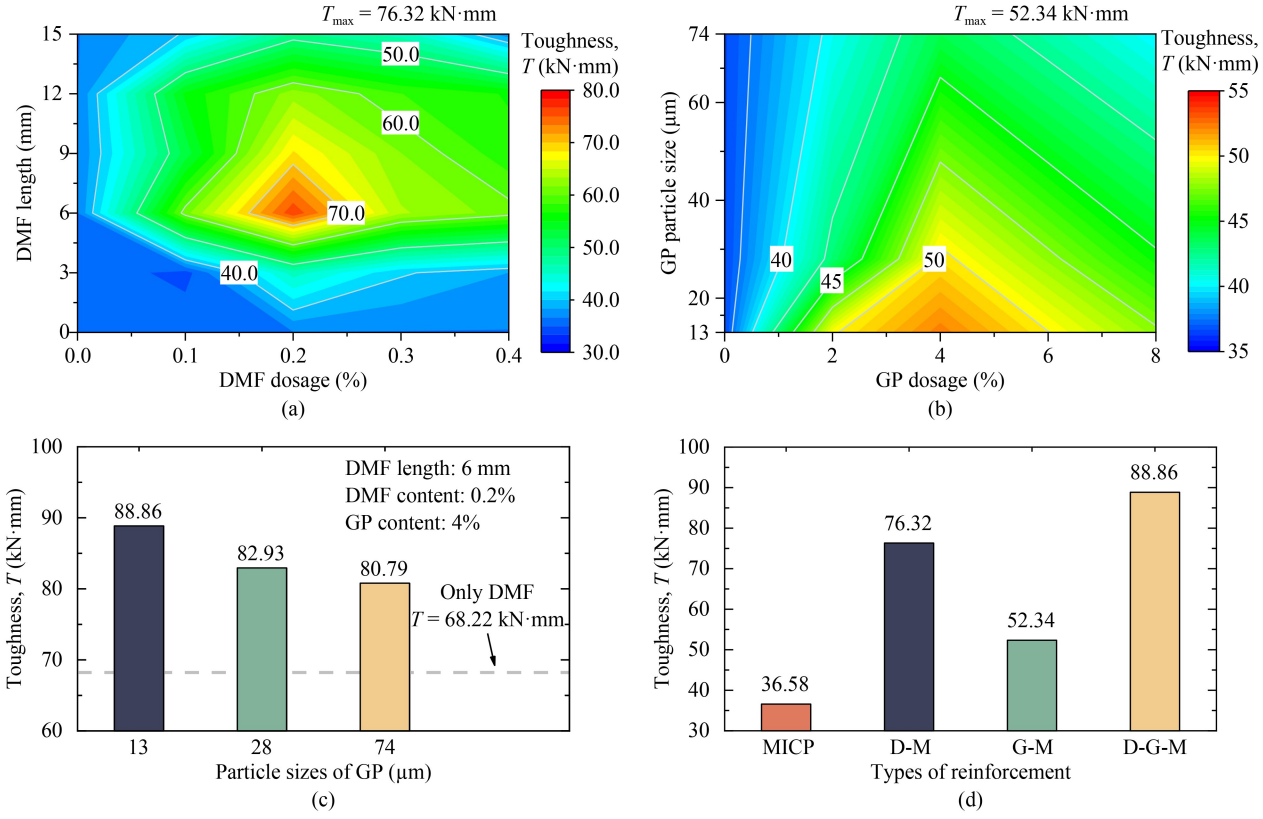

Fig. 8 Effect of incorporation types on toughness index of MICP-treated calcareous sand: (a) D-M group; (b) G-M group; (c) D-G-M group; (d) optimal incorporation results.

For specimens treated exclusively by MICP, the large particle size and high porosity of the calcareous sand resulted in sparsely distributed $CaCO_3$ crystals, primarily located within inter-particle voids (Fig. 9(a)) and adhering to sand grain surfaces. Consequently, effective inter-particle cementation was limited. This observation is attributed to the restricted attachment of microorganisms solely to sand particle surfaces in the only MICP group, leading to a markedly lower BAR relative to groups with admixtures (as discussed in Subsection 3.1).

In the F-M group, as depicted, DMF formed a skeletal network by connecting with sand particles through $CaCO_3$ cementation. The inclusion of DMF enhanced bacterial adsorption and calcium ion utilization efficiency compared to the only MICP group, thereby promoting greater $CaCO_3$ precipitation. Consistent with prior studies, DMF, interacting with microorganisms on sand particle surfaces, directed $CaCO_3$ crystallization to the fiber-sand interface, establishing robust DMF-Sand bridging structures [57]. This mechanism improved the specimens' strength, deformation capacity, and toughness. Notably, the incorporation of 15 mm long fibers led to bending, entanglement, and agglomeration due to their excessive length. Reduced $CaCO_3$ precipitation was observed on fiber surfaces within these agglomerates, diminishing the overall reinforcement efficacy.

The SEM micrograph for the G-M group is presented in Fig. 9(c). GP offered numerous adsorption sites for microorganisms. The subsequently adsorbed bacteria facilitated increased $CaCO_3$ formation, leading to GP-$CaCO_3$ composite structures. These GP-$CaCO_3$ structures optimized the microstructure of the MICP-treated calcareous sand in two principal ways: first, they effectively filled inter-granular pores, significantly enhancing the material's density; second, they promoted uniform $CaCO_3$ deposition across sand particle surfaces, resulting in a more continuous and denser cementation network compared to the only MICP group. Such microstructural enhancements markedly improved the mechanical performance of the calcareous sand, notably its UCS and deformation capacity.

Figure 9(d) reveals the microstructure of specimens from the D-G-M group. GP furnished ample adsorption sites for microorganisms, forming GP-$CaCO_3$ structures with the precipitated calcite. These structures filled voids, increasing soil density and cementation strength. Concurrently, DMF acted as a binding agent, interconnecting the GP-$CaCO_3$ structures, which further augmented the mechanical properties of the composite material.

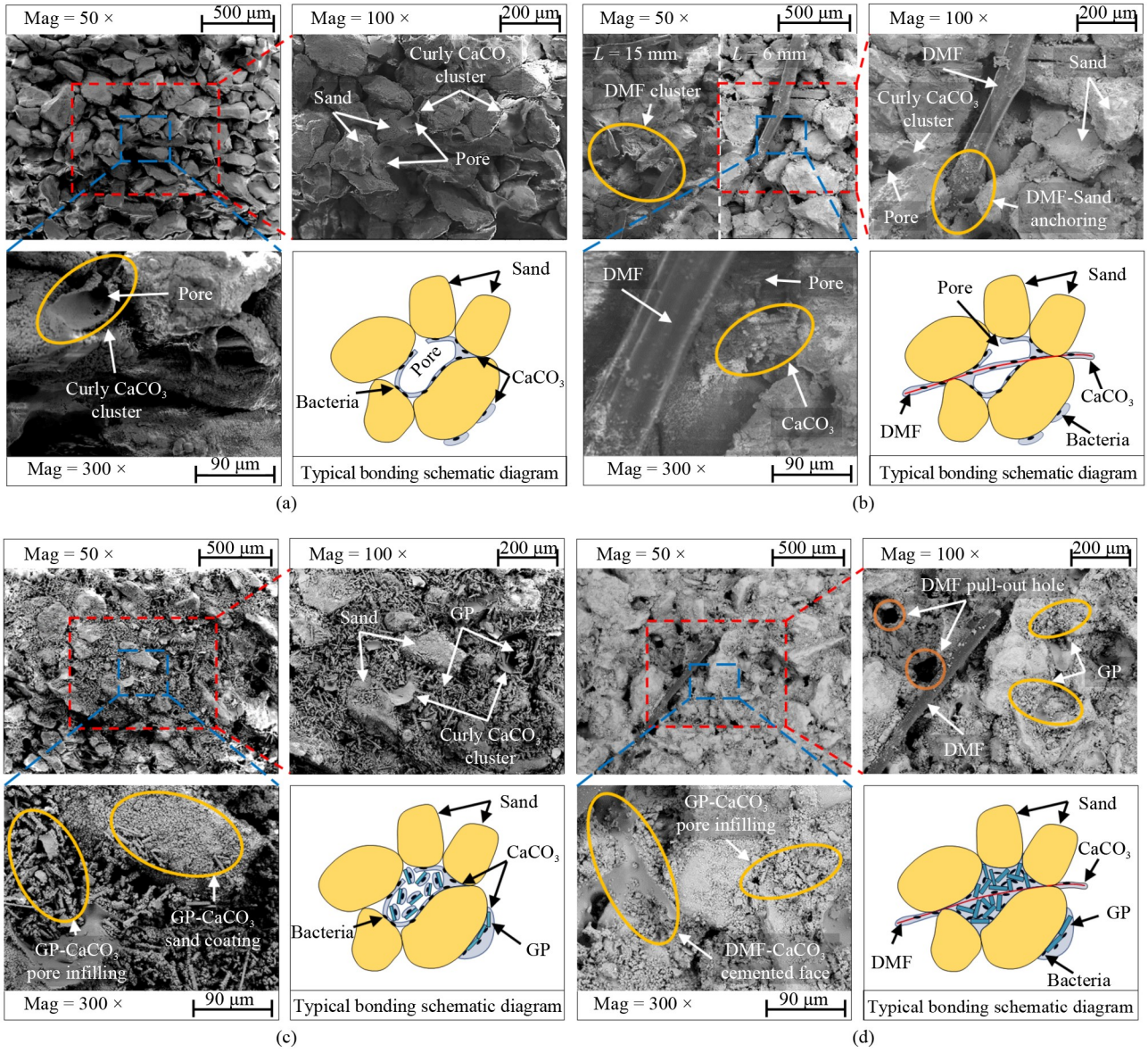

Fig. 9 SEM images of specimens with different reinforcing methods: (a) MICP group; (b) D-M group: 0.2% DMF (6 and 15 mm); (c) G-M group: 4% GP (74 μm); (d) D-G-M group: 4% GP (13 μm) + 0.2% DMF (6 mm).

6 Conclusions

This study proposes a novel composite reinforcement strategy that synergistically integrates MICP with DMF and waste GP. It investigates the effects of these additives on microbial mineralization, mechanical properties, and microstructural evolution of calcareous sand. The main conclusions are as follows.

1) Individual incorporation of DMF or GP enhances bacterial adsorption and Ca^{2+} utilization in MICP, while facilitating the conversion of calcium carbonate to the thermodynamically stable calcite. The combined incorporation further boosts bacterial adsorption and Ca^{2+} utilization and markedly optimizes microbial mineralization efficiency, with the optimal dosage identified as 6 mm 0.2% DMF and 13 μm 4% GP.

2) Individual DMF incorporation induces a deformation-dominated toughening mechanism through fiber bridging, enhancing the sample's deformation capacity. In contrast, individual GP incorporation mainly boosts UCS by filling sand pores, promoting a strength-led toughening mechanism. For combined incorporation, DMF and GP overcome the limitations of individual mechanisms, yielding a rigid-flexible synergy mechanism: DMF's fiber network enhances deformation resistance, while GP's pore-filling reinforces cementation strength. This synergy optimizes mechanical properties, realizing a balance between high strength without brittleness and high toughness without weakness.

3) The lack of microbial adsorption sites in pure calcareous sand leads to $CaCO_3$ cement dominated by porous, discontinuous curled clusters. Individual DMF

incorporation enhances cementation continuity and pore-filling efficiency via the DMF-sand anchorage structure. Individual GP incorporation achieves uniform cementation by filling pores with fine particles, forming a discrete GP-$CaCO_3$ structure. Combined DMF-GP incorporation synergistically integrates these advantages: the discrete GP-$CaCO_3$ structure is tightly linked through DMF's bridging effect, cementing the system into a more robust integral structure.

The synergistic effect resulting from the combined incorporation of DMF and GP overcomes the performance limitations of individual materials through multi-link coupling. This approach offers an efficient and environmentally friendly composite enhancement strategy for the engineering application of MICP technology in calcareous sand reinforcement. Notably, this research is constrained by its focus on short-term mechanical and mineralization properties determined under controlled laboratory settings, thus lacking evaluation of long-term stability against complex environmental stresses. Additionally, given the use of small-scale indoor samples, the adaptability and engineering effectiveness of the optimized scheme must be verified at a larger scale, which points to the primary direction for future research efforts toward practical application.

Acknowledgements We would like to express our thanks to the financial support for this study from the Project of the National Natural Science Foundation of China (Grant Nos. 52108324, 52008207, 52178336, and 52478346) and the Postgraduate Research and Practice Innovation Program of Jiangsu Province (No. KYCX24_1585). The authors would like to render their heartfelt thanks to the anonymous reviewers whose minute and critical review have immensely helped to improve the clarity and quality of the manuscript.

Competing interests The authors declare that they have no competing interests.

References

1. Lv Y R, Li X, Fan C F, Su Y C. Effects of internal pores on the mechanical properties of marine calcareous sand particles. Acta Geotechnica, 2021, 16(10): 3209–3228
2. Lv C, Tang C S, Zhang J Z, Pan X H, Liu H. Effects of calcium sources and magnesium ions on the mechanical behavior of MICP-treated calcareous sand: Experimental evidence and precipitated crystal insights. Acta Geotechnica, 2023, 18(5): 2703–2717
3. Shan Y, Liufu Z Y, Yuan J, Li Y Y, Tong H W, Cui J. Liquefaction resistance of MICP-treated calcareous sand with different particle size and gradation. Biogeotechnics, 2025, 100181
4. Ma G L, Xiao Y, He X, Li J, Chu J, Liu H L. Kaolin-nucleation-based biotreated calcareous sand through unsaturated percolation method. Acta Geotechnica, 2022, 17(8): 3181–3193
5. Ouyang H R, Dai G L, Qin W, Zhang C F, Gong W M. Dynamic behaviors of calcareous sand under repeated one-dimensional impacts. Soil Dynamics and Earthquake Engineering, 2021, 150: 106891
6. Wang X Z, Jiao Y Y, Wang R, Hu M J, Meng Q S, Tan F Y. Engineering characteristics of the calcareous sand in Nansha Islands, South China Sea. Engineering Geology, 2011, 120(1–4): 40–47
7. Wu Y, Li N, Wang X, Cui J, Chen Y, Wu Y, Yamamoto H. Experimental investigation on mechanical behavior and particle crushing of calcareous sand retrieved from South China Sea. Engineering Geology, 2021, 280: 105932
8. Zhang X L, Sun Y, Chen Y M, Liu L, Li W W, Han Y. Uniformity of microbial injection for reinforcing saturated calcareous sand: A multi-test approach. Biogeotechnics, 2025, 3(2): 100105
9. Abo-El-Enein S A, Ali A H, Talkhan F N, Abdel-Gawwad H A. Utilization of microbial induced calcite precipitation for sand consolidation and mortar crack remediation. HBRC Journal, 2012, 8(3): 185–192
10. Chen Y M, Han Y, Zhang X L, Sarajpoor S, Zhang S H, Yao X F. Experimental study on permeability and strength characteristics of MICP-treated calcareous sand. Biogeotechnics, 2023, 1(3): 100034
11. Xiao Y, Hu J, Shi J Q, Zhang L, Liu H L. Undrained cyclic responses of biocemented calcareous silty sand. Acta Geotechnica, 2024, 19(10): 6683–6690
12. Zhou B, Zhang X, Wang J F, Wang H B, Shen J W. Insight into the mechanism of microbially induced carbonate precipitation treatment of bio-improved calcareous sand particles. Acta Geotechnica, 2023, 18(2): 985–999
13. Xu J, Wang X Z, Yao W, Kulminskaya A A, Shah P S. Microbial-inspired self-healing of concrete cracks by sodium silicate-coated recycled concrete aggregates served as bacterial carrier. Frontiers of Structural and Civil Engineering, 2024, 18(1): 14–29
14. Haque M M, Shelote K M, Singh N, Gupta S. Bibliographic survey and comprehensive review on mechanical and durability properties of microorganism based self-healing concrete. Frontiers of Structural and Civil Engineering, 2024, 18(9): 1445–1465
15. Xiao P, Liu H L, Stuedlein A W, Evans T M, Xiao Y. Effect of relative density and biocementation on cyclic response of calcareous sand. Canadian Geotechnical Journal, 2019, 56(12): 1849–1862
16. Xiao Y, He X, Zaman M, Ma G L, Zhao C. Review of strength improvements of biocemented soils. International Journal of Geomechanics, 2022, 22(11): 03122001
17. Liu L, Liu H L, Stuedlein A W, Evans T M, Xiao Y. Strength, stiffness, and microstructure characteristics of biocemented calcareous sand. Canadian Geotechnical Journal, 2019, 56(10): 1502–1513
18. Hu J, Xiao Y, He X, Shi J Q, Liu H L, Chu J. Unified equivalent intergranular void ratio for biotreated binary soils in characterizing liquefaction resistance. Geotechnique, 2025, 75(11): 1485–1501
19. Imran M A, Gowthaman S, Nakashima K, Kawasaki S. The influence of the addition of plant-based natural fibers (Jute) on biocemented sand using MICP method. Materials, 2020, 13(18): 4198
20. Shan Y, Li J W, Zhou H Z, Li Y D, Yuan J, Cui J. Liquefaction resistance of MICP treated silica and calcareous sand with carbon fiber. Acta Geotechnica, 2025, 84: 159

21. Terzis D, Laloui L. Cell-free soil bio-cementation with strength, dilatancy and fabric characterization. Acta Geotechnica, 2019, 14(3): 639–656
22. Salifu E, MacLachlan E, Iyer K R, Knapp C W, Tarantino A. Application of microbially induced calcite precipitation in erosion mitigation and stabilisation of sandy soil foreshore slopes: A preliminary investigation. Engineering Geology, 2016, 201: 96–105
23. Lai H J, Wu S F, Cui M J, Chu J. Recent development in biogeotechnology and its engineering applications. Frontiers of Structural and Civil Engineering, 2021, 15(5): 1073–1096
24. Shukla A K, Sharma A K. Recent developments and future prospects of micro-organisms in enhancement of soil for geotechnical engineering applications: A review. Bioresource Technology Reports, 2024, 28: 101979
25. Xiao Y, He X, Stuedlein A W, Chu J, Evans T M, van Paassen L A. Crystal growth of MICP through microfluidic chip tests. Journal of Geotechnical and Geoenvironmental Engineering, 2022, 148(5): 06022002
26. Zhao C, Xiao Y, Liu H L, Chu J. Effects of urease and cementing solution concentrations on micro-scale enzymatic mineralisation characteristics. Geotechnique, 2025, 75(6): 732–746
27. Banik N, Sarkar R. Effects of bacterial strains on undrained cyclic behavior of bio-cemented sand considering wetting and drying cycles. Journal of Rock Mechanics and Geotechnical Engineering, 2025, 17(1): 432–452
28. Xiao Y, Fu G Y, Shi J Q, Huang X L, Cui H, Liu H L. Bio-hydrogel and biomineralization in improving water retention ability of sandy soils. Acta Geotechnica, 2025, 20(9): 4589–4597
29. Ma G L, Xiao Y, Chu J, Yin Z Y, Zhou B, Liu H L. Pore-scale investigation of MICP in simplified pore structures through microfluidic tests. Water Resources Research, 2025, 61(2): e2024WR037807
30. Zhang J X, Xiao Y, Liu H L, Chu J. Role of bacteria on bio-induced calcium carbonate formation: insights from droplet microfluidic experiments. Geotechnique, 2025, 75(6): 787–799
31. Ahrari M, Karahan M, Hussain M, Nawab Y, Khan A, Shirazi A A. Development of anti-bacterial and anti-viral nonwoven surgical masks for medical applications. Tekstilec, 2022, 65(2): 135–146
32. Ahmed W, Lim C W. Effective recycling of disposable medical face masks for sustainable green concrete via a new fiber hybridization technique. Construction & Building Materials, 2022, 344: 128245
33. Chen S, Zhu Y, He X Y, Su Y, Liu Q, Chen W, Wang Y J, Zhang H Y, Wang W T, Fan J Y et al. Properties of recycled facemask fiber modified asphalt binder: Comparative analysis of surface modification and composite modification method. Construction & Building Materials, 2023, 406: 133466
34. Zhang X S, Wang H Y, Wang Y, Wang J H, Cao J, Zhang G. Improved methods, properties, applications and prospects of microbial induced carbonate precipitation (MICP) treated soil: A review. Biogeotechnics, 2025, 3(1): 100123
35. Bi J, Pan Y X, Mu W X, Yang S, Wang G X, Mao M Y, Wang S N, Wei T T. Predicting the unfrozen water content of freezing soils using an artificial neural network model. Journal of Cold Regions Engineering, 2025, 40(1): 04025050
36. Xiao Y, Zhang L, Shi J, Hu J, Evans T M. Liquefaction of EICP-treated sand with fabric anisotropy. Journal of Geotechnical and Geoenvironmental Engineering, 2025, 152(1): 04025180
37. Han Y, Chen Y M, Chen R Z, Liu H L, Yao X F. Effect of incorporating discarded facial mask fiber on mechanical properties of MICP-treated sand. Construction & Building Materials, 2023, 395: 132299
38. Tang C S, Li H, Pan X H, Yin L Y, Cheng L, Cheng Q, Liu B, Shi B. Coupling effect of biocementation-fiber reinforcement on mechanical behavior of calcareous sand for ocean engineering. Bulletin of Engineering Geology and the Environment, 2022, 81(4): 163
39. Zhao Y, Yang S, Xiao Z, Zhu W, Meng F, Zhang B, Yuan M. Effect of silica powder on microbial-induced carbonate precipitation improvement of medium-coarse sand. Bulletin of Engineering Geology and the Environment, 2023, 82(4): 116
40. Zhao Y, Fan C, Ge F, Cheng X, Liu P. Enhancing strength of MICP-treated sand with scrap of activated carbon-fiber felt. Journal of Materials in Civil Engineering, 2020, 32(4): 04020061
41. ASTM. Standard practice for classification of soils for engineering purposes (unified soil classification system), ASTM D 2487-00. West Conshohocken, PA: American Society for Testing and Materials 2017
42. Hamid A, Ahmad N, Zaidi B, Khalid R A, Hafeez I, Hussain J, Khitab A, Kırgız M S. GlasSphalt: A borosilicate based sustainable engineering material for asphalt pavements. Sustainability, 2023, 15(5): 4277
43. Laurent O, Mantisi B, Micoulaut M. Structure and topology of soda-lime silicate glasses: Implications for window glass. Journal of Physical Chemistry B, 2014, 118(44): 12750–12762
44. Liao M R, Liu H L, Wang X, Hu X Z, Huang Y H, Liu X Q, Brenan K, Mecha J, Nirmalan M, Lu J R. A technical review of face mask wearing in preventing respiratory COVID-19 transmission. Current Opinion in Colloid & Interface Science, 2021, 52: 101417
45. Saberian M, Li J, Kilmartin-Lynch S, Boroujeni M. Repurposing of COVID-19 single-use face masks for pavements base/subbase. Science of the Total Environment, 2021, 769: 145527
46. Li Y J, Guo Z, Wang L Z, Li Y L, Liu Z Y. Shear resistance of MICP cementing material at the interface between calcareous sand and steel. Materials Letters, 2020, 274: 128009
47. Shi L, Qiao H Y, Yang X, Zhang B, Zhang J W. Experimental investigation of fracture permeability reduction process by MICP technology with Sporosarcina pasteurii cultured by different mediums. Acta Geotechnica, 2024, 19(11): 7349–7368
48. Lai Y M, Yu J, Liu S Y, Liu J F, Wang R K, Dong B W. Experimental study to improve the mechanical properties of iron tailings sand by using MICP at low pH. Construction & Building Materials, 2021, 273: 121729
49. Qin J Y, Qin Q Y, Li X G, Xue J X, Wang R Q, Zhang Q, Wang P Q, Guo Z Z, Gong Y F. Urea supply control in microbial carbonate precipitation to effectively fill pores of concrete. Construction & Building Materials, 2021, 310: 125123
50. Zhang Y S, Liu Y, Sun X D, Zeng W, Xing H P, Lin J Z, Kang S B, Yu L. Application of microbially induced calcium carbonate precipitation (MICP) technique in concrete crack repair: A review.

Construction & Building Materials, 2024, 411: 134313
51. Chen M, Gowthaman S, Nakashima K, Komatsu S, Kawasaki S. Used paper fibers for sustainably enhancing the MICP stabilization of sand. In: Kim S S, Moghal A A B, Yao J, eds. Advances in Urban Geotechnical Engineering. Cham: Springer International Publishing, 2021, 52–64
52. Zhao J, Huang G P, Liao L, Liu V W. Appraising the potential of calcium sulfoaluminate cement-based grouts in simulated permafrost environments. Frontiers of Structural and Civil Engineering, 2023, 17(5): 722–731
53. Ghanizadeh A R, Rahrovan M. Modeling of unconfined compressive strength of soil-RAP blend stabilized with portland cement using multivariate adaptive regression spline. Frontiers of Structural and Civil Engineering, 2019, 13(4): 787–799
54. Xu G Y, Fang Y, Zhang Z T, Jiang Y F, Yao Y X, Ying K C, Zhuo B. Experimental study on the hardening behavior of compacted cohesive soil and its rapid evaluation method. Tunnelling and Underground Space Technology, 2026, 168: 107109
55. Espinal M, Kane S, Ryan C, Phillips A, Heveran C. Evaluation of the bonding properties between low-value plastic fibers treated with microbially-induced calcium carbonate precipitation and cement mortar. Construction & Building Materials, 2022, 357: 129331
56. Dong C R, Guo Z, Zhu Y Q, Rui S J, Li Y J. Effect of water glass-enhanced biocementation in sand: Early strength enhancement and mechanistic insights. Construction & Building Materials, 2025, 479: 141516
57. Yang X, Hu Z, Wang Y, Wang X. Aeolian sand stabilized by using fiber- and silt-reinforced cement: Mechanical properties, micro-structure evolution, and reinforcement mechanism. Construction & Building Materials, 2024, 411: 134750